Journal Pre-proof

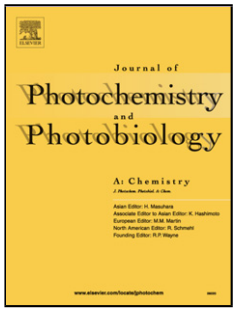

Chelation enhanced fluorescence of rhodamine based novel organic nanoparticles for selective detection of mercury ions in aqueous medium and Intracellular cell imaging

Prasad G. Mahajan, Jin Sik Shin, Nilam C. Dige, Balasaheb D. Vanjare, Yohan Han, Nam Gyu Choi, Song Ja Kim, Sung Yum Seo, Ki Hwan Lee

PII: S1010-6030(20)30378-6

DOI: https://doi.org/10.1016/j.jphotochem.2020.112579

Reference: JPC 112579

To appear in: *Journal of Photochemistry & Photobiology, A: Chemistry*

Received Date: 7 February 2020

Revised Date: 17 April 2020

Accepted Date: 19 April 2020

Please cite this article as: Mahajan PG, Shin JS, Dige NC, Vanjare BD, Han Y, Choi NG, Kim SJ, Seo SY, Lee KH, Chelation enhanced fluorescence of rhodamine based novel organic nanoparticles for selective detection of mercury ions in aqueous medium and Intracellular cell imaging, *Journal of Photochemistry and amp; Photobiology, A: Chemistry* (2020), doi: https://doi.org/10.1016/j.jphotochem.2020.112579

Chelation enhanced fluorescence of rhodamine based novel organic nanoparticles for selective detection of mercury ions in aqueous medium and Intracellular cell imaging

Prasad G. Mahajan[a*], Jin Sik Shin[b], Nilam C. Dige[c], Balasaheb D. Vanjare[a], Yohan Han[c], Nam Gyu Choi[a], Song Ja Kim[c], Sung Yum Seo[c], Ki Hwan Lee[a*]

[a]Department of Chemistry, Kongju National University, Gongju, Chungnam 32588, Republic of Korea.

[b]Department of Chemistry, Chungnam National University, Daejeon 34134, Republic of Korea

[c]Department of Biological Sciences, Kongju National University, Gongju, Chungnam 32588, Republic of Korea.

*Corresponding Email: mahajanprasad2188@gmail.com (P. G. Mahajan); khlee@kongju.ac.kr (K. H. Lee)

Graphical Abstract

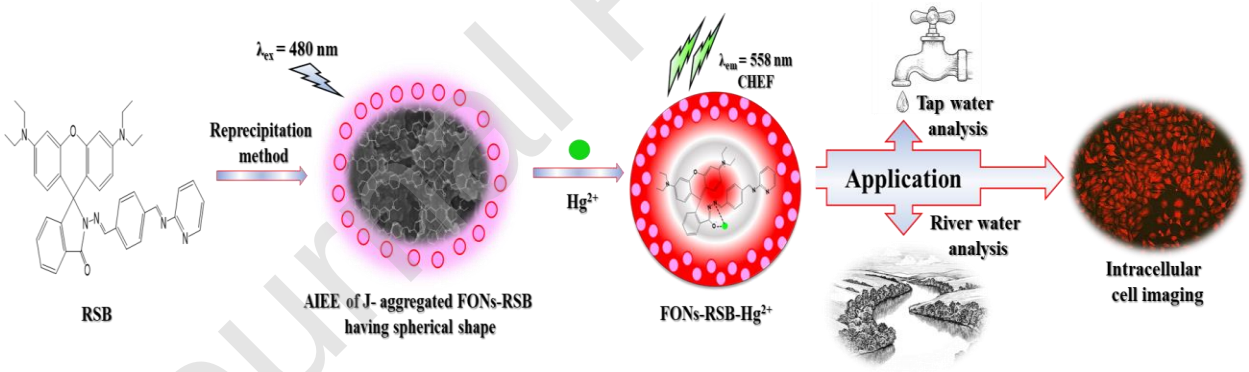

Highlights:

- Fluorescent organic nanoparticles **FONs-RSB** prepared by reprecipitation method
- **FONs-RSB** showed Chelation enhanced fluorescence only in the presence of Hg^{2+}
- Interference-free detection of Hg^{2+} ions using a proposed sensing method

- The extremely low detection limit of 1.729 ng/mL for Hg^{2+} ions in an aqueous medium
- Feasibilities are analysis of environmental samples and intracellular cell imaging

Abstract

A simple, quick and useful reprecipitation method was used to prepare rhodamine based fluorescent nanoparticles. The characterization techniques such as zeta-particle sizer and scanning electron microscopy were studied to investigate the formation of desired nanoparticles **FONs-RSB** along with its aqueous stability, surface charge, particle size, and morphological features. The comparative optical properties between parent molecule RSB and **FONs-RSB** were examined using absorption and fluorescence studies. The sphere morphology of **FONs-RSB** having 82 nm particle size and negative zeta potential (-33.5 mV) showed selective and sensitive interaction with only Hg^{2+} amongst the series of metal ion studied which was revealed by florescence titration results. The interaction between **FONs-RSB** and Hg^{2+} leads to enhance the fluorescence of **FONs-RSB** is because of chelation enhanced fluorescence (CHEF) phenomenon. The interference of foreign metal ions was found to be unaffected to the fluorescence enhancement induced by Hg^{2+}. The binding stoichiometry and binding constant were evaluated using Job's and modified Benesi-Hildebrand plot. The mechanism of binding interaction and nature of complexation were analyzed using Infrared (IR), Nuclear Magnetic Resonance (NMR), absorption and fluorescence lifetime titrations in the absence and presence of a variable amount of Hg^{2+} to **FONs-RSB**. Further, the reaction product of the sensing process in the present investigation was examined using mass analysis. The detection limits calculated using the present method were found to be 1.729 ng/mL (8.619 nM) and 1.68 ng/mL when linear concentration of Hg^{2+} additions were 0-2 µg/mL and 0-100 ng/mL, respectively. The practical application of the present method involves the quantitative determination of Hg^{2+}

in environmental samples collected from the local campus and intracellular cell imaging of Hg^{2+} using A375 living cells with non-toxic behavior.

Keywords: Rhodamine based fluorescent organic nanoparticles; Mercury ions; Chelation enhanced fluorescence; Environmental samples; Cell imaging.

1. Introduction:

Pollution occurred by contamination of heavy metal ions in the aquatic and biological systems increased day by day. Concerning about the hazardous effects arises from heavy metal ions to human being demands acute, rapid, selective and sensitive method for their qualitative and quantitative determination. The intake of heavy metals ions is essential for the human body at certain levels to maintain the biological and therapeutic balance in the function of various processes associated with the human body [1-3]. One of the toxic and unsafe heavy metal ions is mercury (Hg^{2+}). Mercury originates in the forms of three groups such as Hg, Hg^{+} and Hg^{2+}. Among these three groups, mercury in its divalent oxidation state (Hg^{2+}) is most toxic due to its mobility in the living systems and ability to cross cell membranes [4-5]. The mining water, power plants, household bleaches, fungicides, petrochemicals and chemicals including acids are the main sources through which mercury has potency to release in the environment [6-8]. The severe threats to human health arise due to the variable concentration of Hg^{2+} in the body and which can be enriched through the food chain and cause harmful effects on human health [9-10]. It affects and damages central nervous system, kidneys, digestive system, lungs and immune system and further led to increase risk level of hypertension, oxidative stress and anemia [10-12]. Therefore, continuous research on detection and reduction of Hg^{2+} pollution in aquatic and biological systems increases nowadays in science and engineering society.

Numerous analytical techniques have been devoted to examining the Hg^{2+} concentration in aqueous system. These techniques include atomic emission spectroscopy (AES) [13], stripping voltammetry [14], atomic fluorescence spectroscopy (AFS) [15],

Inductively coupled plasma mass spectroscopy (ICP-MS) [16], electrochemical sensors [17], fluorometric methods [18,19], cold vapor atomic fluorescence (CV-AFS) [20], polarography [21], colorimetric analyzes [22] and inductively coupled plasma-atomic emission spectroscopy [23]. Amongst these immense varieties of analytical methods for the determination of Hg^{2+} concentration in environmental samples, most are costly, time-consuming, requires pre-sample treatments, fail to produce extremely low detection limit and needs sample storage during analysis. These drawbacks encourage to expand sensing method for qualitative and quantitative determination of Hg^{2+} in environmental samples which needs economical, rapid, selective, sensitive and low detection level approach. In an addition, there were number of probes have been used to monitor Hg^{2+} such as proteins, cells, nanomaterials, organic fluorophores, polymers, chromophores and DNA based molecules [24]. Interestingly, rhodamine based organic fluorophores have been devotedly used for detection of heavy metal ions due to their spirolactum ring opening and fluorescence turn-ON characteristics [25-28]. Additionally, considering the design of nanomaterial-based on rhodamine core will have extra-ordinary properties as compared to their parent compound in the organic solvent and may use for sensing purpose of heavy metal ions in aqueous medium at ultra-trace levels, an attempt was made for the preparation of their fluorescent organic nanoparticles for their sensing application in the present studies.

Currently, one of the swiftly expanding research areas is nanomaterials which offer remarkable benefits in biological sciences, health sciences and medical engineering [3,4]. There are various many research groups on the development of fluorescent chemosensors for sensitive detection of metal ions in aqueous medium [1-4]. Traditional fluorescence-based chemosensors used for the detection of an analyte in aqueous media bears disadvantages in comparison with the nanomaterials. Such chemosensors are highly hydrophobic and most of the time were used in organic solvents or mixed organic solvent systems which may lead to produce interferences from foreign analytes, fail to producing low detection limits, lack sensitivity, and selectivity. To overcome these shortcomings, fluorescence-based organic nanoparticles (FONs) become the most capable candidature to analyze the analyte of interest from the aqueous medium without interferences of other

analytes with an extremely low detection limit [29-31]. The ease of synthesis, real-time qualitative and quantitative analysis, high surface to volume ratio, extra-ordinary photophysical properties, sensitivity and selectivity towards analyte of interest, no interference from other existing or competing analytes and capacity to have an extremely low detection limit of analyte are the noticeable advantages of fluorescence-based organic nanoparticles. The increasing industrial and mining activities throughout the whole population raises the risk of health hazards produced by increasing level of Hg^{2+} contamination in ecological system. Therefore, to reduce such health risk of Hg^{2+} pollution, demands development of selective, sensitive and low cost effective analytical method for its acute determination in aqueous medium which can be achieved employing design, preparation and use of fluorescence-based organic nanoparticles (FONs) for heavy metal ion sensing.

In the present study, we have designed rhodamine Schiff base cored organic molecule 3',6'-bis(diethylamino)-2-((E)-4-((E)-(pyridin-2-ylimino)methyl)benzylidene-amino)spiro[isoindoline-1,9'-xanthen]-3-one *i.e.* **RSB** which was further used to prepare fluorescent organic nanoparticles (**FONs-RSB**) using the reprecipitation method. The sensing studies reveals **FONs-RSB** can effectively and selectively interacts with only Hg^{2+} amongst the series of heavy metal ion. The interaction between **FONs-RSB** and Hg^{2+} led to produce selective chelation enhanced fluorescence in **FONs-RSB** while other metal ions produces negligible effects. The present fluorescence-based analytical method provides a simple, rapid, sensitive and selective quantitative approach for the determination of Hg^{2+} in environmental samples collected from the local area. The extremely low detection of Hg^{2+} concentration at the nano and micro-level can be possible by using the present analytical approach. Additionally, the prepared nanoparticles showed non-toxic behavior towards human malignant melanoma A375 cell line. Subsequently, the intracellular detection of Hg^{2+} using **FONs-RSB** is an additional benefit of prepared nanoparticles which will explore its potent application in the biomedical field.

2. Experimental: Materials and methods:

2.1 Materials:

Rhodamine B, Terephthalaldehyde, hydrazine hydrate, concentrated sulfuric acid and 2-amino pyridine were procured from Alfa Aesar. The solvents of analytical grade such as methanol, ethanol and acetone used in the present study were purchased from Samchun chemicals, Korea and used without further purification. All the metal ion solutions were prepared by using their salts which were obtained from Alfa Aesar. Double distilled water used in the series of experiments was collected from Milli-Q system. The 5-dimethylthiazol-2-yl-2,5-diphenyltetrazoliumbromide (MTT) was obtained from Sigma Aldrich. The human malignant melanoma A375 cell line and Fetal bovine serum (FBS) with Dulbecco modified eagle medium (DMEM) were received from Korean Cell Line Bank (KCLB), Seoul, South Korea and Gibco (Carlsbad, CA, USA), respectively.

2.2 Methods:

2.2.1 Synthesis of 3',6'-bis(diethylamino)-2-((E)-4-((E)-(pyridin-2-ylimino)methyl)-benzylideneamino)spiro[isoindoline-1,9'-xanthen]-3-one (RSB):

100 mL round bottom flask equipped with rhodamine B (5 mmol, 2.39 g), 50 mL ethanol and 3 mL concentrated sulfuric acid (H_2SO_4) was vigorously stirred for 6 h at room temperature. The formation of rhodamine B ester was monitored on thin layer chromatography (TLC) progress after specific reaction time. After completion of reaction, the mixture was allowed to evaporate under reduced pressure to remove excess quantity of ethanol. To the received crude solid compound (rhodamine B ester), excess quantity of hydrazine hydrate (1 mL, 20 mmol) and solvent as 10 mL methanol were added. The whole reaction mass was further stirred for the period of 4 h at room temperature. The progress of reaction and formation of the compound - rhodamine B hydrazide were monitored on TLC. Thereafter, reaction mixture was evaporated on rotary using vacuum pressure technique. Thus, slight pink colored solid received was recrystallized using hot ethanol. The recrystallized rhodamine B hydrazide was received in appreciable yield of 89% (2.031 g), which was further used for the preparation of compound **RSB**.

To prepare compound **RSB**, rhodamine B hydrazide (2 mmol, 0.913 g) was poured into 25 mL round bottom flask containing 5 mL methanol and allowed to stir at room temperature. The successive addition of terephthalaldehyde (2 mmol, 0.268 g) was done and allow the reaction mixture to stir for next 1 h. Afterwards, 2-amino pyridine (2 mmol, 0.188 g) was added to the reaction mixture. The complete reaction mixture was permitted to stir at room temperature till the completion of reaction and aldehyde became completely consumed. The consumption of reactants into formation of desired compound **RSB** was examined on TLC. After 8 h, the reaction mixture shows completion of reaction into new product *i.e.* **RSB**. The crushed ice was added to the reaction mass and stirred vigorously for next 30 min. The slight pink colored solid crude compound thus obtained was filtered and washed with distilled water. The purification of compound **RSB** was done using recrystallization process in hot ethanol. The recrystallized product of compound **RSB** thus received was in satisfactory yield of 85% (1.103 g). **Scheme 1** illustrates schematic representation of approach for the synthesis of **RSB**. The recrystallized compound **RSB** further used for the spectral characterization such as IR, NMR and Mass analysis followed by preparation of fluorescent organic nanoparticles of **RSB** *i.e.* **FONs-RSB**.

2.2.1.1 Spectral Characterization of compound RSB:

Melting point (M.P.): Observed: 189-191 ^{0}C; IR (**Fig. S1**): 2923, 2603, 1715 (-C=O), 1637 (-C=N), 1590 (-C=N), 1539, 1455, 1382, 1312, 1267, 1167, 1133, 1116, 1082, 1055, 999, 919, 850, 824, 755, 705, 665 cm^{-1}; ^{1}H-NMR(600 MHz, DMSO-d_6) (**Fig. S2**): δ 8.93 (s, 1H,=CH), 8.79 (s, 1H,=CH), 7.87 – 7.94 (m, 3H, ArH), 7.56 – 7.66 (m, 4H, ArH), 7.36 (s, 1H, ArH), 7.10 – 7.14 (m, 2H, ArH), 6.43 – 6.47 (m, 3H, ArH), 6.41 – 6.43 (t, 1H, ArH), 6.38 – 6.39 (d, 1H, ArH), 6.30 – 6.35 (m, 3H, ArH), 3.28 – 3.31 (q, 8H, -CH_2), 1.05 – 1.09 (t, 12H, -CH_3,) ppm; ^{13}C-NMR(150 MHz, DMSO-d_6) (**Fig. S3**) : δ 193.08, 164.55, 153.56, 151.60, 149.11, 146.17, 130.74, 128.03, 127.80, 108.31, 105.82, 98.22, 43.93, 12.53 ppm; LCMS (ESI) (**Fig. S4**): 649.4 [M+1] m/z.

2.2.2 Preparation of fluorescent organic nanoparticles of RSB (FONs-RSB):

A simply operative reprecipitation method was used for the preparation of aqueous suspension of fluorescent organic nanoparticles of **RSB** [29-31]. For this purpose, 0.5 mL, 10×10^{-3} M RSB in acetone was swiftly injected using micro syringe into beaker containing 100 mL of double distilled water. The solution was stirred vigorously on magnetic stirrer for 45 min followed by 15 min sonication at 30 °C. The colorless aqueous suspension of nanoparticles **FONs-RSB** (50×10^{-6} M) thus obtained was further used to investigate the physical, morphological, optical and sensing properties.

2.2.3 Characterization techniques:

Frontier IR (Perkin Elmer) spectrometer was procured for the purpose of scanning the FT-IR spectrum. The Bruker Avance 600 MHz spectrometer (Germany) with TMS as an internal standard was used to perform examination of ^{1}H NMR and ^{13}C NMR spectra. The LC-MS spectra were analyzed on 2795/ZQ2000 (waters) spectrometer and Bruker MicroTof-Q spectrometer (Germany). The particle size and charge over the surface of prepared nanoparticles were measured by Dynamic light scattering (DLS) technique using Malvern Zeta - Particle size analyzer. The FE-SEM (MIRA3 LMH, TESCAN, USA) was utilized for investigation of morphology of prepared nanoparticles. The Shimadzu (Japan) spectrophotometer and FS-2 fluorescence spectrophotometer (Scinco, Korea) were used to examine the changes observed in UV–visible (absorption) and fluorescence spectra in corresponding solvents. The fluorescence lifetime decay performance of **FONs-RSB** in the presence and absence of Hg^{2+} ion was evaluated on time correlated single photon counting (TCSPC) Spectrophotometer (HORIBA-iHR320, Japan) at its excitation wavelength. Thus, received outputs were analyzed on Data station software equipped with the instrument for the estimation of fluorescence lifetime values of **FONs-RSB** in the presence and absence of Hg^{2+}.

2.2.4 Cell culture and fluorescence imaging:

The A375 cells were grown in DMEM medium using 10% FBS, penicillin (50 units/mL) and streptomycin (50 µg/mL). The A375 cells were seeded at the density 1×10^5 cells in 35 mm culture plate. The cells were grown until it reaches 60% by following the treatment of fresh medium every day. Later, A375 cells in respective medium were preserved without (Control) and with RSB in acetone, aqueous suspension of **FONs-RSB** and FONs-RSB + Hg^{2+} ion at particular concentration of 1 µg/mL and 2 µg/mL for 6 h. The cells were washed by cold PBS buffer solution for two times. Further, inverted fluorescence microscope (BX51, Olympus, Tokyo, Japan) under green light was used to examine the treated cells for fluorescence images. The experiment was carried out three times at optimized conditions such as constant exposure time, contrast and brightness settings in humidified atmosphere (95% air and 5% CO_2) at 37 °C in CO_2 incubator.

2.2.5 Viability assay (MTT):

The A375 cells were plated at a density of 2.5×10^4 cells/well on 96-well plates followed by incubation overnight. The cells were supplied with fresh medium on each day until they grown 60%. Thus, such cells were treated without (Control) and with RSB in acetone, aqueous suspension of **FONs-RSB** and FONs-RSB + Hg^{2+} ion at particular concentration. Finally, warm PBS was used to wash cells for two times followed by addition of 90 µL of fresh medium and 10 µL of MTT reagent 1 (MTT, 10 mg/mL) to each sample well. Further, these cells were incubated for next 24 h with the addition of 100 µL of MTT reagent 2 (Solubilisation buffer, 10% SDS with 0.01N HCl and DMSO) at 37 °C in 5% CO_2 incubator. Lastly, the cell viability in the form of absorbance was measured, recorded, and compared with 100% control for each sample on enzyme-linked immunosorbent assay (ELISA) plate at 595 nm.

3. Results and Discussion:

3.1 Effect of pH on fluorescence of FONs-RSB:

The fluorescence performance of any probe can be variable in the presence of different pH environment. Therefore, it is essential to examine and optimize the pH effect for the fluorescence intensity of **FONs-RSB**. In this study, the fluorescence intensity of **FONs-**

RSB was tested in the presence of different pH solution from 1 to 12. The fluorescence intensity at respective pH was plotted and given as **Fig. S5**. It was noticed that fluorescence intensity of **FONs-RSB** found to be maximum at neutral pH = 7. The decrease in the fluorescence intensity at acidic and basic conditions was attributed to disruption of structural cavity of nanoparticles followed by aggregation [31-33]. The neutral pH plays significantly vital role in the biological experiments. Therefore, neutral pH =7 was optimized for each solution during further experiments.

3.2 Particle size distribution, Zeta potential and Morphology of FONs-RSB:

The particle size distribution curve of **FONs-RSB** is given as **Fig. 1**. The analysis of particle size illustrates narrow distribution of **FONs-RSB** within the range of 60-150 nm having average particle size of 82 nm. To investigate the charge over the surface of **FONs-RSB**, zeta potential was examined. **Fig. 2** represents the zeta potential curve for prepared **FONs-RSB**. The value of zeta (ζ) potential -33.5 mV indicates the superior aqueous stability of **FONs-RSB**. It is well known that aqueous suspension of nanoparticles having either high negative or positive zeta potential value is electrically stabilized [34]. In addition, the negative zeta potential value of **FONs-RSB** shows negative charge lies over the surface of nanoparticles. Such negative charge over the prepared nanoparticles **FONs-RSB** can be further utilized to examine the sensing ability with oppositely charged metal ions or analytes in aqueous medium. To investigate the morphological aspects, the scanning electron microscopy (SEM) was used. **Fig. 3** indicates scanning electron microphotograph of **FONs-RSB**, which clearly shows the distinct sphere shape morphology for the prepared nanoparticles. The average particle size estimated through SEM analysis was found to be 100-120 nm which is in close agreement with the particle size analyzed using DLS technique (**Fig.1**). The rationale behind the observation of large particle size during SEM analysis is aggregation of **FONs-RSB** while making air -dried film due to repeatedly injecting aqueous suspension of nanoparticles on glass substrate in order to have thin film.

3.3 Absorption and fluorescence studies:

It is well known that optical properties such as absorption, fluorescence and fluorescence lifetime of nanoparticles are much more significantly distinct than those of parent molecules. Therefore, to recognize the separate identity of nanoparticles than that of monomer (parent molecule), absorption and fluorescence spectra followed by estimation of fluorescence lifetime values in respective solvents were performed. **Fig. 4** shows absorption spectrum of RSB in acetone (A) and aqueous suspension of **FONs-RSB** (B). The absorption spectrum clearly indicates nanoparticles shown their variable character as compared with the parent molecule via bathochromically shifting of absorption band. The distinct absorption band at 420 nm and less pronounced band at 376 nm for RSB in acetone are assigned to n-π* and π-π* electronic transitions, respectively. In case of nanoparticles (**FONs-RSB**), these absorption bands are found to be bathochromically shifted to the maximum wavelength of 418 nm (π-π*) and 509 nm (n-π*). The structural rearrangement *via* head to tail patterns generally known as J- aggregation [35-38] is the reason for shifting of absorption maxima of parent molecule (RSB) to longer wavelength in **FONs-RSB**. The fluorescence spectra of RSB in acetone (A) and aqueous suspension of **FONs-RSB** (B) is given as **Fig. 5**. The excitation wavelength of 420 and 480 nm was used to scan the fluorescence emission spectrum of RSB in acetone and aqueous suspension of **FONs-RSB**, respectively. The broad fluorescence emission peak at 524 nm for RSB in acetone found to be shifted to the longer wavelength at 558 nm which is assigned to aqueous suspension of **FONs-RSB**. Also, 3-fold increase in the fluorescence intensity of **FONs-RSB** than the RSB in acetone indicates aggregation induced enhanced emission (AIEE) phenomenon [36,39]. Such AIEE observed in case of **FONs-RSB** is because of shifting of zeroth vibrational level of ground electronic state to higher excited state in RSB molecule during the formation of J- aggregated nanoparticles *i.e.* **FONs-RSB**. The superior photophysical properties of **FONs-RSB** was also supported by evaluating the fluorescence quantum yield, Stokes shift and fluorescence lifetime values. The estimated fluorescence quantum yield values for FONs-RSB and RSB in acetone were found to be 4.23 and 1.89, respectively. The calculated fluorescence quantum yields suggest **FONs-RSB** are more bright and photophysically active component as compared with RSB in acetone. The estimated Stokes

shift values shows higher value for **FONs-RSB** (1725.55 cm^{-1}) than that of RSB in acetone (1189.69 cm^{-1}) which is in support of formation of **FONs-RSB**. The larger Stokes shift value of **FONs-RSB** also supports the origin of bathochromically shifted AIEE of **FONs-RSB** due to fluorescence emission from lower lying excited state of J- aggregation of RSB molecules. The average time spend by any fluorescent molecule in its excited state is known as fluorescence lifetime of that material. In present case, **FONs-RSB** (5.63 ns) illustrates longer fluorescence lifetime value than parent molecule RSB in acetone (2.11 ns). The observation of longer lifetime value for **FONs-RSB** is attributed to J- aggregates of nanoparticles, which is responsible to restrict the molecular and vibrational rotations in RSB molecules [35-38].

3.4 Chelation enhanced fluorescence enhancement of FONs-RSB:

The functionality present in the RSB molecule and negative charge over the surface of nanoparticles encourage us to examine sensing property of prepared **FONs-RSB** with positively charged metal ion solutions. The metal ion solutions (2 μg/mL) of Hg^{2+}, Ag^{+}, Na^{+}, Fe^{2+}, Ni^{2+}, Pb^{2+}, Al^{3+}, Zn^{2+}, Ba^{2+}, Mn^{2+}, Cu^{2+}, NH_4^{+}, K^{+}, Ca^{2+}, Mg^{2+}, Cd^{2+}, Cr^{3+} and Co^{2+} was added to the aqueous suspension of **FONs-RSB** and further examined for their fluorescence emission response at excitation of 480 nm. **Fig. 6** indicates fluorescence emission spectra of **FONs-RSB** in the presence and absence of variety of positively charged metal ions solution having concentration of 2 μg/mL each. The fluorescence emission of **FONs-RSB** is remained constant or slight variable when metal ions except Hg^{2+} are added to aqueous suspension of **FONs-RSB**. While, addition of Hg^{2+} solution distinctly increases the fluorescence emission of **FONs-RSB** by nearly 7 times more than its initial value. Such increase in the fluorescence emission intensity of **FONs-RSB** by the addition of Hg^{2+} is due to the chelation enhanced fluorescence (CHEF) phenomenon [30,31,41,42]. The opening of spirolactum ring of rhodamine core led to generate more reactive imine (-C=N) group locate near the spirolactum ring of rhodamine and oxygen ($-O^{-}$) of carbonyl group. These functionalities are strongly interacting with the Hg^{2+} ion and

simultaneously increases the rigidity of molecular assembly through restriction of free rotations of carbonyl and imine groups which is resulting in CHEF. In comparison, the sensing ability of parent molecule RSB was also investigated in the presence of a series of metal ions having a concentration of 2 μg/mL each (**Fig. S6**). The parent molecule is highly hydrophobic and hence the sensing experiment was carried out with 10×10^{-3} M RSB in an acetone solution. Interestingly, the sensing property of RSB also tends towards interaction with the Hg^{2+} only but at less extends. After the addition of Hg^{2+} to the solution of RSB in acetone failed to produce enhanced fluorescence for a longer time. Such output received through sensing ability of parent molecule RSB may not able to produce satisfactory detection limits at extremely low levels. Hence, it was concluded that being of hydrophilic characteristics, aqueous stability, ability to produce extremely low detection limits, practical applicability in aqueous systems, selective and sensitive sensing properties for **FONs-RSB** would be the preferred choice for the further investigation through present studies. In addition, the response time is an essential parameter for fluorescent sensors and which was systematically checked by observing fluorescence intensity as a function of response time in minutes and given as **Fig. S7**. The figure illustrates that after the addition of 2 μg/mL of Hg^{2+} to the aqueous suspension of **FONs-RSB**, fluorescence intensity gradually increases till 5 min and further remains constant for the period of 20 min. This clearly indicates **FONs-RSB** is able to sensitize Hg^{2+} within a short period of time and remain invariable during the sensing process. Additionally, the change in the fluorescence intensity was checked after the variation of pH for **FONs-RSB** when in contact with a higher concentration of Hg^{2+} (2 μg/mL). The results are given as supporting information in **Fig. S8**. The maximum fluorescence intensity was observed at neutral pH 7 indicates good stability of formed complexation between **FONs-RSB** and Hg^{2+} through sensing process. This experimental observation clarifies the applicability of **FONs-RSB** would be possible to detect Hg^{2+} in biological samples at an ideal neutral pH range.

3.5 Effect of foreign metal ions:

The selective and sensitive nature for fluorescence enhancement of **FONs-RSB** by the addition of Hg^{2+} was further examined and supported by performing the effect of foreign

metal ion on the performance of fluorescence intensity induced by Hg^{2+} to **FONs-RSB**. The respective solutions of **FONs-RSB** with Hg^{2+} (2 μg/mL) and each foreign metal ion (2 μg/mL) were prepared and scanned for the fluorescence measurement. **Fig. 7** illustrates the change in the fluorescence intensity of **FONs-RSB** in the presence of each metal ion (green color bars) and in the presence of Hg^{2+} along with foreign metal ions (brown color bars). It is observed that only Hg^{2+} can selectively and sensitively enhances the fluorescence intensity of **FONs-RSB** through CHEF process. While, other metal ions failed to produce significant change in the fluorescence intensity of **FONs-RSB**. Interestingly, the study on the effect of foreign metal indicates selective interaction of only Hg^{2+} ion with **FONs-RSB** and could not interfere and affect the detection of Hg^{2+} by the addition of other analytes.

3.6 Estimation of statistical parameters:

3.6.1 Fluorescence titration and Limit of detection:

Fig. 8 shows fluorescence intensity of **FONs-RSB** in the absence and presence of variable concentration of Hg^{2+} ion from 0 to 2 μg/mL. The results show that progressively change in intensity of fluorescence emission of **FONs-RSB** with increase in the concentration of Hg^{2+} solution. This increasing pattern of fluorescence intensity was found to be linear in the concentration range of 0-2 μg/mL of Hg^{2+} solution. The results were plotted as a change in the fluorescence intensity from its initial value to the addition of Hg^{2+} versus the particular concentration of added Hg^{2+} in **FONs-RSB** and used as calibration plot given as **Fig. 9**. The results of the fluorescence enhancement of **FONs-RSB** due to the chelation process were found to be well fitted into a straight line equation in the linear range. The limit of detection (LOD) [42] was evaluated using **equation 1** given below,

$$LOD = \frac{3.3\sigma}{K} \quad (1)$$

In the above equation, σ and K represents the standard deviation of blank measurement and the slope value of the regression line, respectively. The detection limit calculated for Hg^{2+} using the present analytical approach is found to be 1.729 ng/mL (8.619 nM). To verify the detection limit of the present investigation at the nano level, the sensing experiment of

FONs-RSB was carried out at the linear concentration range of 0-100 ng/mL Hg^{2+} solution. **Fig. S9** shows the linear response for change in the fluorescence intensity of **FONs-RSB** at the respective Hg^{2+} concentration. The limit of detection was calculated (1.689 ng/mL) which was found to be in agreement with experimental set up when the concentration of Hg^{2+} with a linear range 0-2 μg/mL. This proves the sensitivity of the proposed analytical approach for micro as well as the nano level concentration of the analyte of interest. The present analytical approach based on rhodamine cored fluorescent nanoparticles for the detection of Hg^{2+} provides appreciably much lower detection limit in addition to practical applicability than the already reported sensors and other analytical techniques. **Table 1** summarizes comparison syntax of proposed fluorescent nanoprobe with already reported analytical methods and probes followed by their applicability in the determination of Hg^{2+}.

3.6.2 Evaluation of binding stoichiometry and binding constant for complexation between FONs-RSB and Hg^{2+}:

The renowned Job's method [30,43,44] was applied to evaluate the binding stoichiometry between complex formation of **FONs-RSB** and Hg^{2+}. The solutions containing varying mole fractions of Hg^{2+} from 0.1 to 0.9 were subjected to examine their absorption and fluorescence spectrum. The total sum of concentration of **FONs-RSB** and Hg^{2+} was kept constant with only changing the mole fraction of Hg^{2+} from 0.1 to 0.9. **Fig. 10** represents as Job's plot shows the respective value of absorption and fluorescence intensity for each of solution holding mole fraction of 0.1 to 0.9 Hg^{2+} ion. The maximum absorption value and fluorescence emission intensity noticed only after the mole fraction of Hg^{2+} achieves a value of 0.5, which signifies the binding stoichiometry between **FONs-RSB** and Hg^{2+} ion could be 1:1. The value of binding constant for complexation between **FONs-RSB** and Hg^{2+} was evaluated using modified Benesi-Hilderbrand (B-H) equation [30,31,45] and given as **equation 2**,

$$\frac{1}{I-I_0} = \frac{1}{(I_{MAX}-I_0)} + \frac{1}{K_B(I_{MAX}-I_0)}\frac{1}{[Hg^{2+}]^n} \qquad (2)$$

In **equation 2**, the maximum fluorescence intensity of **FONs-RSB** in the presence of Hg^{2+}, initial fluorescence intensity of **FONs-RSB** and fluorescence intensity of **FONs-RSB** at

respective concentration of Hg^{2+} is represented as I_{max}, I_0 and I, respectively. While, K_B and n stands for the binding constant and number of Hg^{2+} bound per **FONs-RSB** *i.e.* 1, respectively. The value of binding constant between complexation of **FONs-RSB** with Hg^{2+} was calculated using slope value of modified B-H plot given as **Fig. 11**. The estimated binding constant value (K_B) for 1:1 complexation between **FONs-RSB** and Hg^{2+} in aqueous medium is found to be 4.149×10^3. The considerably higher binding constant value supports sensible binding interactions between **FONs-RSB** and Hg^{2+}.

3.7 Mechanism of chelation enhanced fluorescence of FONs-RSB by Hg^{2+}:

The recent reports were witnessed to recommend the chelation enhanced fluorescence phenomenon through spirolactum ring opening mechanism in case of rhodamine derivatives. To investigate the mechanism of chelation enhanced fluorescence of **FONs-RSB** by the addition of Hg^{2+}, systematic experiments such as analysis of mass spectrum of product formation in sensing process, absorption titration, fluorescence lifetime, zeta-particle size analysis, IR titration and NMR titration were performed in the absence and presence of variable concentration of Hg^{2+}. The sample used for the IR, NMR and Mass analysis was the one which showed maximum absorbance and fluorescence response in experiment of Job's plot and illustrates 1:1 complexation between **FONs-RSB** and Hg^{2+}. The spirolactam ring opening of rhodamine derivative RSB after the addition of Hg^{2+} leads to interact metal ion with functionalities namely carbonyl oxygen (O^-) and nitrogen of imine (-C=N) as shown in **Scheme 2**. The enhanced fluorescence of **FONs-RSB** by Hg^{2+} may be assigned to the conformational rigidification imposed on the nano probe upon metal ion complexation. Such interactions simultaneously restrict the free rotations of carbonyl and imine groups leading to sensitization and chelation induced fluorescence enhancement in presence of Hg^{2+}. The titration results of IR and NMR of **FONs-RSB** in presence of Hg^{2+} are given as supporting information (**Fig. S10** and **Fig. S11**). From the IR spectrum, it seems that shifting of IR stretching frequency of imines from 1590 to 1605 cm^{-1} and 1637 to 1690 cm^{-1} along with disappearance of stretching frequency of the carbonyl group (1705 cm^{-1}) clearly indicates the participation of one of imine group which locates near to spirolactum ring and carbonyl group in the chelation and interaction with Hg^{2+}. These

observations further supported by NMR titration results. The appearance of two singlet peaks at δ 8.93 and δ 8.79 for the proton belongs to imines (HC=N) in NMR spectrum (**Fig. S2**) shows only one singlet peak at δ 9.61 after the addition of Hg^{2+} (**Fig. S11**). The singlet peak observed is assigned to imine group which locates near to pyridine moiety. While, relevant peak positions (δ values) of other protons in molecules are slightly shifted to either downfield or upfield. Hence, IR and NMR titration of **FONs-RSB** with Hg^{2+} suggests interaction patterns and supports chelation enhanced fluorescence mechanism. Further, the product formation of the sensing process was investigated through the Mass analysis. **Fig. S12** given as supporting information shows the mass spectrum of the product of the present sensing process. The found molecular weight (849.1) of the product of the sensing process through the complexation between **FONs-RSB** and Hg^{2+} was in harmony with the expected molecular weight (849.28). This observation suggests the complexation between **FONs-RSB** and Hg^{2+} at 1:1 equivalent ratio. Additionally, the complexation between nanoparticles and Hg^{2+} was confirmed by examining the zeta-particle size results (**Fig. S13**). The zeta potential and particle size were analyzed in the presence of variable concentration of Hg^{2+} (0.5, 1 and 2 μg/mL) to the aqueous suspension of **FONs-RSB**. There is no change observed in case of zeta potential value but increase in only particle size from 82 nm to 468 nm. This observation suggests the complexation between **FONs-RSB** with good aqueous stability. The absorption spectra of **FONs-RSB** in the absence and presence of Hg^{2+} (0 to 2 μg/mL) were examined and results interpret as **Fig. S14**. The bathochromic shift of 23 nm in the absorption maximum wavelength and change in the absorption value after the successful addition of Hg^{2+} from concentration of 0 to 2 μg/mL ignores the possibility of ground state complexation and endorses excited state complexation between **FONs-RSB** and Hg^{2+}. The excited state complexation of FONs-RSB-Hg^{2+} was further supported by analyzing the fluorescence lifetime values in the absence and presence of different concentration of Hg^{2+} to the aqueous suspension of **FONs-RSB**. The rise in the fluorescence lifetime value from 5.63 ns to 6.12 ns after the addition of Hg^{2+} solution having 0 to 2 μg/mL concentration indicates strongly excited state complexation between **FONs-RSB** and Hg^{2+} in an aqueous medium. **Table 2** indicates the fluorescence lifetime

values of **FONs-RSB** in the absence and presence of particular concentration of Hg^{2+} solution. Thus, chelation induced excited state complex of **FONs-RSB-Hg^{2+}** remains longer in the singlet excited state and fluoresces through an increase in the pathways which results in an enhancement in fluorescence of **FONs-RSB** when in contact with the respective concentration of Hg^{2+} solution. **Scheme 2** shows a pictorial representation of a plausible mechanism for the formation of **FONs-RSB** and its interaction with Hg^{2+}.

3.8 Application of proposed fluorescence method:

3.8.1 Quantitative determination of Hg^{2+} in environmental samples using FONs-RSB:

The quantitative determination of Hg^{2+} from collected environmental samples using prepared **FONs-RSB** is the main advantage of proposed analytical method. The samples under studies were processed for filtration and boiling to remove the solid impurities and dissolved gases, if any. The solutions were prepared by spiking known quantity of desired concentration of standard Hg^{2+} solution followed by dilution with respective environmental samples. The calibration plot as given in **Fig. 9** was used to find out the recovery of spiked concentration of Hg^{2+} ion. Pleasingly, observed concentrations of Hg^{2+} are in harmony with the spiked concentrations of Hg^{2+} to the said samples. The obtained data is interpreted in **Table 3**. Hence, proposed fluorescence based analytical approach can be successfully utilized to estimate the Hg^{2+} quantity in an aqueous medium without interference of foreign analytes.

3.8.2 Intracellular cell imaging of Hg^{2+} using FONs-RSB and cell toxicity studies:

The intake of Hg^{2+} in human body severely affects body organs such as kidney, liver, brain, etc. Therefore, it is an essential to develop suitable probe which can selectively and sensitively detects intracellular Hg^{2+} in cell line. Inspired from the enhanced fluorescence properties of **FONs-RSB** when in contact with Hg^{2+}, we performed fluorescence based cell imaging experiment of proposed sensing method using the human malignant melanoma A375 cell line. The cultured cells were subjected to treat with the RSB in acetone, aqueous suspension of **FONs-RSB** and FONs-RSB + Hg^{2+} ion at particular concentration. The fluorescence images for cell imaging studies were scanned at excitation wavelength of 532

nm and given as **Fig. 12**. It was found that, RSB in acetone (**Fig. 12, S2**) showed very fragile fluorescence when in contact with the human malignant melanoma A375 cell line. While, **FONs-RSB** (**Fig. 12, S3**) displayed enhanced fluorescence in cell imaging. Interestingly, intracellular fluorescence of **FONs-RSB** was further increased (**Fig. 12, S4** and **S5**) when foreign metal ion Hg^{2+} of concentration 1 μg/mL (**Fig. 12, S4**) and 2 μg/mL (**Fig. 12, S5**) was externally added to the human malignant melanoma A375 cell line. **Fig. 13** illustrates cell viability of A375 cells cultured in complete media with RSB in acetone, aqueous suspension of **FONs-RSB** and FONs-RSB + Hg^{2+} ion at particular concentration. The MTT assay [46] was performed to check the cytotoxicity effects on A375 cells after 24 h of prepared samples treatments. Satisfyingly, the desired nanoprobe **FONs-RSB** and its complex form with Hg^{2+} were found to be non-toxic with A375 cells. Hence, it was concluded that prepared rhodamine cored fluorescent organic nanoparticles **FONs-RSB** could be the best choice for intracellular detection of Hg^{2+}.

4. Conclusion:

Rhodamine based compound (RSB) was synthesized and characterized at the molecular scale. The fluorescent organic nanoparticles of RSB (**FONs-RSB**) were prepared by using the reprecipitation method. The nano-level particle size of 82 nm and sphere shape morphology were examined on the particle size analyzer and scanning electron microscope, respectively. The functionalities present in the molecule and negative charge over the surface of **FONs-RSB** suggested examining the fluorescence response in the presence of a variety of metal ions to evaluate the sensing ability of prepared nanoparticles. Pleasingly, only Hg^{2+} ion induced chelation enhanced fluorescence in **FONs-RSB**, while other metal ions respond negligibly. Additionally, none of foreign metal ion interferences in the selective and sensitive detection of Hg^{2+} in an aqueous medium using **FONs-RSB**. The fluorescence enhancement of **FONs-RSB** was found to be linear in the concentration range of 0-2 μg/mL of Hg^{2+}. The excited state 1:1 complexation through chelation of Hg^{2+} with **FONs-RSB** was supported by studies on IR, NMR, absorption and fluorescence lifetime titrations. The formation of complexation *i.e.* sensing product was confirmed by analysis

of mass spectrum of 1:1 equivalent of **FONs-RSB** and Hg^{2+}. The limit of detection (LOD) for Hg^{2+} is found to be 1.729 ng/mL (8.619 nM) using proposed method and which is superior than probes and methods reported earlier. The present fluorescence based analytical method provides simple, rapid, sensitive and selective quantitative approach for the determination of Hg^{2+} in environmental samples. The intracellular detection of Hg^{2+} using **FONs-RSB** is an additional benefit of prepared nanoparticles which will explore its potent application in biomedical field.

Conflict of Interest:

Authors declare no conflict of interest.

Author Statement

We are submitting herewith our revised research article entitled, **"Chelation enhanced fluorescence of rhodamine based novel organic nanoparticles for selective detection of mercury ions in aqueous medium and Intracellular cell imaging"** for consideration and publication in your reputed Journal, "**Journal of Photochemistry and Photobiology A: Chemistry**".

We hereby give the warranty that the manuscript submitted to the journal for review is original, and has not been published elsewhere; is not currently being considered for publication by any other journal and will not be submitted for such review while under review by the Journal "**Journal of Photochemistry and Photobiology A: Chemistry**".

Declaration of Interest Statement

Authors declare no conflict of interest.

Acknowledgements

This research was supported by Basic Science Research Program through the National Research Foundation of Korea (NRF) funded by the Ministry of Education (NRF- 2019R1I1A3A01059089).

References:

1. S. Sarkar, T. Mondal, S. Roy, R. Saha, A.K. Ghosh, S.S. Panja, A multi-responsive thiosemicarbazone-based probe for detection and discrimination of group 12 metal ions and its application in logic gates, New J. Chem. 42 (2018) 15157–15169.

2. (a) P . Miao , L . Liu, Y . Li, G. X. Li, A novel electrochmical method to detect mercury (II) ions, Electrochem. commun. 11 (2009) 1904–1907.; (b) P. G. Mahajan, N. C. Dige, N. K. Desai, S. R. Patil, V. V. Kondalkar, S. K. Hong, K. H. Lee, Selective detection of Co^{2+} by fluorescent nano probe: Diagnostic approach for analysis of environmental samples and biological activities, Spectrochim. Acta A 198 (2018) 136–144.

3. (a) Y. Ding, Y. Tang, W. Zhu, Y. Xie, Fluorescent and colorimetric ion probes based on conjugated oligopyrroles, Chem. Soc. Rev. 44 (2015) 1101-1112.; (b) Y. Ding, W. Zhu, Y. Xie, Development of Ion Chemosensors Based on Porphyrin Analogues, Chem. Rev. 117 (2017) 2203-2256.

4. M. Lufti Firdaus, I. Fitriani, S. Wyantuti, Y. W. Hartati, R. Khaydarov, J. A. Mcalister, H. Obata, T. Gamo, Colorimetric Detection of Mercury (II) ion in aqueous solution using silver nanoparticles, Anal. Sciences. 33 (2017) 831-837.

5. M. Harada, Minamata disease: methylmercury poisoning in Japan caused by environmental pollution, Crit. Rev. Toxicol., 25 (1995) 1-24.

6. A. Gopalakrishna, T. V. Pavan Kumar, Intravenous injection of elemental mercury: A report of two cases, Indian J. Plast. Surg. 41 (2008) 214–218.

7. N. A. Azmi, S. H. Ahmad, S. C. Low, Detection of mercury ions in water using a membrane-based colorimetric sensor, RSC Adv. 8 (2018) 251–261.

8. B. V. Tangahu, S. R. Sheikh Abdullah, H. Basri, M. Idris, N. Anuar, M. Mukhlisin, A Review on Heavy Metals (As, Pb, and Hg) Uptake by Plants through Phytoremediation, Int. J. Chem. Eng. 2011 (2011) DOI:10.1155/2011/939161.

9. (a) G. Zeng, C. Zhang, D. Huang, C. Lai, L. Tang, Y. Zhou, P. Xu, H. Wang, L. Qin, M. Cheng, Practical and regenerable electrochemical aptasensor based on nanoporous gold and thymine-Hg^{2+}-thymine base pairs for Hg^{2+} detection, Biosens. Bioelectron. 90 (2017) 542-548; (b) C. Lai, S. Liu, C. Zhang, G. Zeng, D. Haung, L. Qin, X. Liu, H. Yi, R. Wang, F. Huang, B. Li, T. Hu, Electrochemical Aptasensor Based on Sulfur-Nitrogen Codoped Ordered Mesoporous Carbon and Thymine-Hg^{2+}-Thymine Mismatch Structure for Hg^{2+} Detection, ACS Sens. 3 (2018) 2566-2573.

10. (a) L. Cherian, V. K. Gupta, A simple field test for the detection of mercury in polluted water, air and soil samples, Fresenius J. Anal. Chem. 336 (1990) 400-402.; (b) F. Zahir, S. J. Rizwi, S. K. Haq, R. H. Khan, Low dose mercury toxicity and human health, Environ. Toxicol. Pharacol. 20 (2005) 351–360.

11. P. Holmes, K. A. James, L.S. Levy, Is low-level environmental mercury exposure of concern to human health? Sci. Total Environ. 408 (2009) 171-182.

12. E. M. Nolan, S. J. Lippard, Tools and tactics for the optical detection of mercuric ion, Chem. Rev. 108 (2008) 3443-3480.

13. F. X. Han, W. Dean Patterson, Y. J. Xia, B. B. Maruthi Sridhar, Y. J. Su, Rapid determination of mercury in plant and soil samples using inductively coupled plasma atomic emission spectroscopy, a comparative study, Water Air Soil Pollut. 170 (2006) 161-171.

14. P. Ugo, L.M. Moretto, P. Bertoncello, J. Wang, Determination of trace mercury in saltwater at screen-printed electrodes modified with sumichelate Q10R, Electroanalysis 10 (1998) 1017–1021.

15. L. P. Yu, X. P. Yan, Flow injection on-line sorption preconcentration coupled with cold vapor atomic fluorescence spectrometry and on-line oxidative elution for the determination of trace mercury in water samples, Atomic Spectroscopy 25 (2004) 145–153.

16. J. S. D. Santos, M. D. L. Guárdia, A. Pastor, M.L.P.D. Santos, Determination of organic and inorganic mercury species in water and sediment samples by HPLC on-line coupled with ICP-MS, Talanta 80 (2009) 207-211.

17. M. P. Gilad, T. V. Ran, J. Elbaz, I. Willner, Nanoengineered electrically contacted enzymes on DNA scaffolds: functional assemblies for the selective analysis of Hg^{2+} ions, J. Am. Chem.Soc. 132 (2010) 6878-6879.

18. W. Lu, X. Qin, S. Liu, G. Chang, Y. Zhang, Y. Luo, A. M. Asiri, A. O. Al-Youbi, X. Sun, Economical, green synthesis of fluorescent carbon nanoparticles and their use as probes for sensitive and selective detection of mercury (II) ions, Anal. Chem. 84, (2012) 5351-5357.

19. K. D. Bhatt, D. J. Vyas, B. A. Makwana, S. M. Darjee, V. K. Jain, H. Shah, Turn-on fluorescence probe for selective detection of Hg(II) by calixpyrrole hydrazide reduced silver nanoparticle: application to real water sample, Chin. Chem. Lett. 27 (2016) 731–737.

20. H. Bagheri, A. Gholami, Determination of very low levels of dissolved mercury(II) and methylmercury in river waters by continuous flow with on-line UV decomposition and cold-vapor atomic fluorescence spectrometry after pre-concentration on a silica gel-2-mercaptobenzimidazol sorbent, Talanta 55 (2001) 1141-1150.

21. L. N. Suvarapu, S. O. Baek, Recent studies on the speciation and determination of mercury in different environmental matrices using various analytical techniques, Int. J. Anal. Chem. 2017 (2017) DOI:10.1155/2017/3624015.

22. L. S. Walekar, A. H. Gore, P. V. Anbhule, V. Sudarsan, S. R. Patil, G. B. Kolekar, A novel colorimetric probe for highly selective recognition of Hg^{2+} ions in aqueous media based on inducing the aggregation of CPB-capped AgNPs: accelerating direct detection for environmental analysis, Anal. Methods 5 (2013) 5501–5507.

23. C. A. Trimble, R. W. Hoenstine, A. B. Highley, J. F. Donoghue, P. C. Ragland, Baseline sediment trace metals investigation: Steinhatchee river estuary, Florida, Northeast Gulf of Mexico, Mar. Georesour. Geotechnol. 17 (1999) 187-197.

24. L. H. Jin, C. S. Han, Eco-friendly colorimetric detection of mercury (II) ions using label-free anisotropic nanogolds in ascorbic acid solution, Sensors and Actuators B 195 (2014) 239-245.

25. H. N. Kim, M. H. Lee, H. J. Kim, J. S. Kim, A new trend in rhodamine-based chemosensors: application of spirolactam ring-opening to sensing ions Chem. Soc. Rev. 37 (2008) 1465–1472.

26. X. Chen, T. Pradhan, F. Wang, J. S. Kim, J. Yoon, Fluorescent chemosensors based on spiroring-opening of xanthenes and related derivatives, Chem. Rev. 112 (2012) 1910–1956.

27. M. Saleem, R. Abdullah, A. Ali, B. J. Park, E. H. Choi, I. S. Hong, K. H. Lee, Synthesis, cytotoxicity and bioimaging of a novel Hg^{2+} selective fluorogenic chemosensor, Anal. Methods 6 (2014) 3588-3597.

28. F. Yan, D. Cao, N. Yang, Q. Yu, M. Wang, L. Chen, Sens. Actuators B 162 (2012) 313–320.

29. P. G. Mahajan, N. C. Dige, B. D. Vanjare, S. H. Eo, S. J. Kim, K. H. Lee, A nano sensor for sensitive and selective detection of Cu^{2+} based on fluorescein: cell imaging and drinking water analysis, Spectrochim. Acta A. Mol. Biomol. Spectrosc. 216 (2019) 105–116.

30. P. G. Mahajan, N. C. Dige, B. D. Vanjare, Y. Han, S. J. Kim, S. K. Hong, K. H. Lee, Intracellular imaging of zinc ion in living cells by fluorescein based organic nanoparticles, Sens. Actuators B Chem. 267 (2018) 119–128.

31. P. G. Mahajan, D. P. Bhopate, G. B. Kolekar, S. R. Patil, N-methyl isatin nanoparticles as a novel probe for selective detection of Cd^{2+} ion in aqueous medium based on chelation

enhanced fluorescence and application to environmental sample, Sens. Actuators B Chem. 220 (2015) 864–872.

32. L. Wang, L. Wang, L. Dong, G. Bian, T. Xia, H. Chen, Direct fluorimetric determination of γ-globulin in human serum with organic nanoparticle biosensor, Spectrochim. Acta A 61 (2005) 129–133.

33. P. G. Mahajan, N. K. Desai, D. K. Dalavi, D. P. Bhopate, G. B. Kolekar, S. R. Patil, Cetyltrimethylammonium bromide capped 9-anthraldehyde nanoparticles for selective recognition of phosphate anion in aqueous solution based on fluorescence quenching and application for analysis of chloroquine, J. Fluoresc. 25 (2015) 31–38.

34. J. Lyklema, Fundamentals of Interface and Colloid Science, Elsevier, Wageningen, (1995)

35. F. Wang, M. Han, M. Yi, Y. Wang, Y. Lai, Aggregation driven growth of size-tunable organic nanoparticles using electronically altered conjugated polymers, J. Am. Chem. Soc. 127 (2005) 10350–10355.

36. P. G. Mahajan, G. B. Kolekar, S. R. Patil, Recognition of D-penicillamine using Schiff base centered fluorescent organic nanoparticles and application to medicine analysis, J. Fluoresc. 27 (2017) 829–839.

37. X. Zhang, X. Zhang, S. Wang, M. Liu, L. Tao, Y. Wei, Surfactant modification of aggregation-induced emission material as biocompatible nanoparticles: facile preparation and cell imaging, Nanoscale 5 (2013) 147–150.

38. P. G. Mahajan, D. P. Bhopate, G. B. Kolekar, S. R. Patil, FRET sensor for erythrosine dye based on organic nanoparticles: application to analysis of food stuff, J. Fluoresc. 26 (2016) 1467–1478.

39. D. K. Dalavi, D. P. Bhopate, A. S. Bagawan, A. H. Gore, N. K. Desai, A. A. Kamble, P. G. Mahajan, G. B. Kolekar, S. R. Patil, Fluorescence quenching studies of CTAB

stabilized perylene nanoparticles for the determination of Cr(VI) from environmental samples: spectroscopic approach, Anal. Methods 6 (2014) 6948–6955.

40. M. Kumar, A. Kumar, M. Kumar Singh, S.K. Sahu, R.P. John, A novel benzidine based Schiff base turn-on fluorescent chemosensor for selective recognition of Zn^{2+}, Sens. Actuators B 241 (2017) 1218–1223.

41. L. N. Wang, W. W. Qin, W. S. Liu, A sensitive Schiff-base fluorescent indicator for the detection of Zn^{2+}, Inorg. Chem. Commun. 13 (2010) 1122–1125.

42. P. G. Mahajan, N. C. Dige, S. B. Suryawanshi, D. K. Dalavi, A. A. Kamble, D. P. Bhopate, A. N. Kadam, V. V. Kondalkar, G. B. Kolekar, S. R. Patil, FRET between Riboflavin and 9-Anthraldehyde based fluorescent organic nanoparticles possessing Antibacterial activity, J. Fluoresc. 28 (2018) 207–215.

43. A. Samanta, N. Guchhaitb, S. C. Bhattacharya, A simple but highly selective and sensitive fluorescence reporter for toxic Cd (II) ion via excimer formation, Chem. Phy. Lett. 612 (2014) 251–255.

44. P. Job, Formation and stability of inorganic complexes in solution, Ann. Chim. 9 (1928) 113–203.

45. H. A. Benesi, J. H. Hildebrand, A spectrophotometric investigation of the interaction of iodine with aromatic hydrocarbons, J. Am. Chem. Soc. 71 (1949) 2703–2707.

46. A. R. Phull, M. Majid, I. U. Haq, M. R. Khan, S. J. Kim, In vitro and in vivo evaluation of anti-arthritic, antioxidant efficacy of fucoidan from Undaria pinnatifida (Harvey) Suringar, Int. J. Biol. Macromol. 97 (2017) 468–480.

47. H. E. Kaoutit, P. Estevez, F. Garcia, F. Serna, J. M. Garcia, Sub-ppm quantification of Hg(II) in aqueous media using both the naked eye and digital information from pictures of a colorimetric sensory polymer membrane taken with the digital camera of a conventional mobile phone, Anal. Methods, 5 (2013) 54–58.

48. G. H. Chen, W. Y. Chen, Y. C. Yen, C. W. Wang, H. T. Chang, C. F. Chen, Detection of Mercury(II) Ions Using Colorimetric Gold Nanoparticles on Paper-Based Analytical Devices, Anal. Chem. 86 (2014) 6843-6849.

49. Y. Yang, Z. Wang, M. Yang, M. Zhaoyang, W. Guoli, S. R. Yu, Inhibitive determination of mercury ion using a renewable urea biosensor based on self-assembled gold nanoparticles, Sensors and Actuators B 114 (2006) 1–8.

50. N. R. Devi, M. Sasidharan, A. K. Sundramoorthy, Gold Nanoparticles-Thiol Functionalized Reduced Graphene Oxide Coated Electrochemical Sensor System for Selective Detection of Mercury Ion, Journal of The Electrochemical Society, 165 (2018) B3046-B3053.

51. A. Samphao, H. Rerkchai, J. Jitcharoen, D. Nacapricha, K. Kalcher, Indirect Determination of Mercury by Inhibition of Glucose Oxidase Immobilized on a Carbon Paste Electrode, Int. J. Electrochem. Sci. 7 (2012) 1001–1010.

52. O. O. Soldatkin, I. S. Kucherenko, V. M. Pyeshkova, A. L. Kukla, N. Jaffrezic-Renault, A. V. Eliskaya, S. V. Dzyadevych, A. P. Soldatkin, Novel conductometric biosensor based on three-enzyme system for selectivedetermination of heavy metal ions, Bioelectrochemistry 83 (2012) 25–30.

53. N. Zohora, D. Kumar, M. Yazdani, V. M. Rotello, R. Ramanathan, V. Bansal, Rapid colorimetric detection of mercury using biosynthesized gold nanoparticles, Colloids and Surfaces A 532 (2017) 451–457.

54. X. Zeng, J. Liu, Z. Zhang, S. Kong, Sensitive and Selective Detection of Mercury Ions by Potentiometric Biosensor Based on Urease Immobilized in Chitosan–Poly(Vinyl Alcohol) Hydrogel Film, Int. J. Electrochem. Sci. 10 (2015) 8344 - 8352

55. E. Coronado, J. R. Galain-Mascarois, C. Marti-Gastaldo, E. Palomares, J. R. Durrant, R. Vilar, M. Gratzel, M. K. Nazeeruddin, Reversible Colorimetric Probes for Mercury Sensing, J. Am. Chem. Soc. 127 (2005) 12351-12356.

56. T. K. Krawczyk, M. Moszczyniska, M. Trojanowicz, Inhibitive determination of mercury and other metal ions bypotentiometric urea biosensor, Biosensors & Bioelectronics 15 (2000) 681 – 691.

57. J. Do, K. Lin, R. Ohara, Preparation of urease/nano-structured polyaniline-Nafion1/Au/Al_2O_3 electrode for inhibitive detection of mercury ion, J. Taiwan Institute of Chem. Engi. 42 (2011) 662–668.

58. Y. C. Hsieh, J. L. Chir, H. H. Wu, P. S. Chang, A. T. Wu, A sugar-aza-crown ether-based fluorescent sensor for Hg^{2+} and Cu+, Carbohydrate Research 344 (2009) 2236–2239.

59. P. G. Mahajan, N. C. Dige, B. D. Vanjare, A. R. Phull, S. Ja Kim, K. H. Lee, Gallotannin mediated silver colloidal nanoparticles as multifunctional nano platform: Rapid colorimetric and turn-on fluorescent sensor for Hg^{2+}, catalytic and In vitro anticancer activities, J. Lumin. 206 (2019) 624–633.

60. D. Hu, Z. Sheng, P. Gong, P. Zhang, L. Cai, Highly selective fluorescent sensors for Hg^{2+} based on bovine serum albumin-capped gold nanoclusters, Analyst 135 (2010) 1411–1416.

61. P. Ncube, R. W. M. Krause, D. T. Ndinteh, B. B Mamba, Fluorescent sensing and determination of mercury (II) ions in water, Water SA 40 (2014) 175-182.

62. Y. Li-Rong, L. Kai-Bin, Y. Xing, Z. Rong-Bin, H. Zheng, p-Dimethylamino-benzaldehyde thiosemicarbazone: A simple novelselective and sensitive fluorescent sensor for mercury(II)in aqueous solution, Talanta 69 (2006) 103–106.

63. C. Huang, Z. Yang, K. Lee, H. Chang, Synthesis of Highly Fluorescent Gold Nanoparticles for Sensing Mercury(II), Angew. Chem. Int. Ed. 46 (2007) 6824-6828.

Scheme captions:

Scheme 1: Synthetic route of RSB

Scheme 2: Pictorial presentation of plausible mechanism for the formation of **FONs-RSB** and its interaction with Hg^{2+}

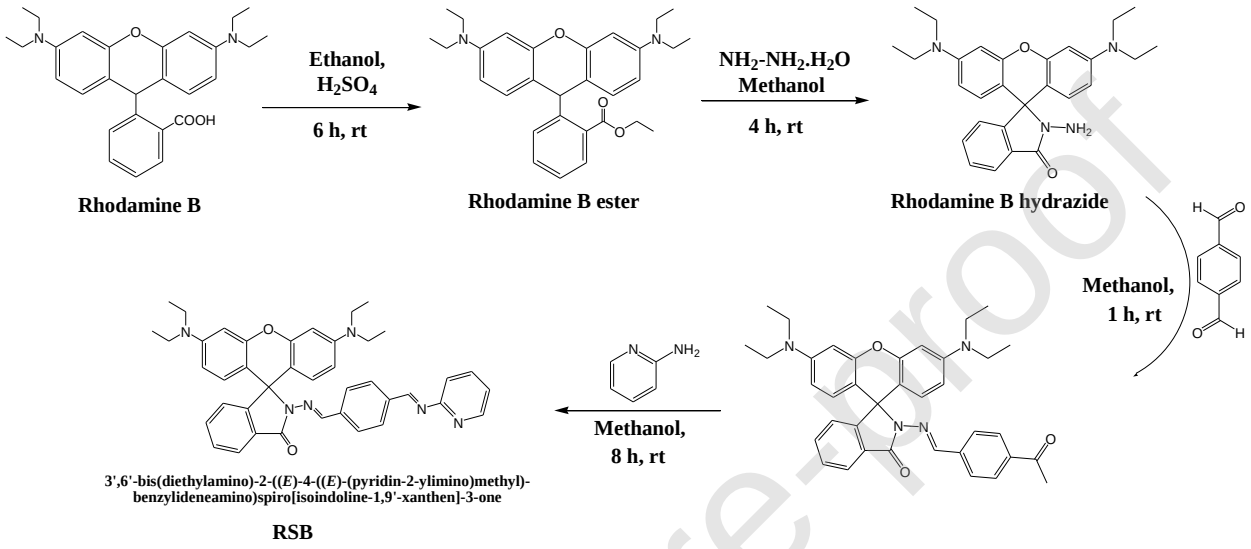

Scheme 1: Synthetic route of RSB

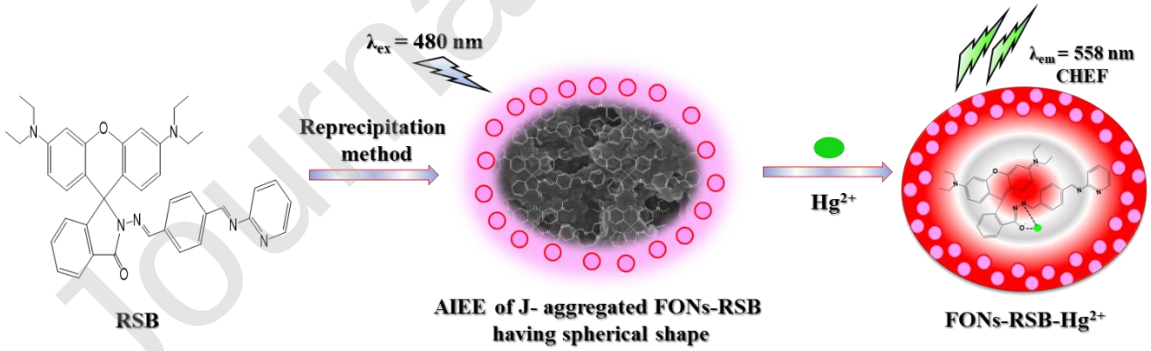

Scheme 2: Pictorial presentation of plausible mechanism for the formation of **FONs-RSB** and its interaction with Hg^{2+}

Figure captions:

Fig. 1: Particle size distribution curve of **FONs-RSB**

Fig. 2: zeta potential curve of **FON-RSB**

Fig. 3: Scanning electron microphotograph of **FONs-RSB**

Fig. 4: Absorption spectrum of RSB in acetone [10 mM] (A) and aqueous suspension of **FONs-RSB** [50 μM] (B)

Fig. 5: Fluorescence spectra of RSB in acetone [10 mM] (A) and aqueous suspension of **FONs-RSB** [50 μM] (B)

Fig. 6: Fluorescence emission spectra of **FONs-RSB** [50 μM] in the presence and absence of variety of positively charged metal ion solution [2 μg/mL]

Fig. 7: Impact on change in the fluorescence intensity of **FONs-RSB** [50 μM] in the presence of each metal ion (green color bars, 2 μg/mL) and in the presence of Hg^{2+} along with foreign metal ions (brown color bars, 2 μg/mL)

Fig. 8: Fluorescence intensity of **FONs-RSB** [50 μM] in the absence and presence of variable concentration of Hg^{2+} ion from 0 to 2 μg/mL

Fig. 9: Calibration plot for fluorescence enhancement of **FONs-RSB** [50 μM] by Hg^{2+} addition [0-2 μg/mL]

Fig. 10: Job's plot to investigate binding stoichiometry between **FONs-RSB** and Hg^{2+}

Fig. 11: Modified Benesi-Hildebrand Job's plot

Fig. 12: Bright filed transmission images, fluorescence images exposed in green light 532 nm and merge images of living A375 cells with control (S1), RSB in acetone (S2) [10 mM], FONs-RSB (S3) [50 μM], FONs + 1 μg/mL Hg^{2+} (S4) and FONs-RSB + 2 μg/mL Hg^{2+} (S5)

Fig. 13: Cell viability measurement using the MTT assay. A375 cells were untreated (Control-S1) and cells treated with RSB in acetone (S2) [10 mM], FONs-RSB (S3) [50 μM], FONs + 1 μg/mL Hg^{2+} (S4) and FONs-RSB + 2 μg/mL Hg^{2+} (S5) for 24 h.

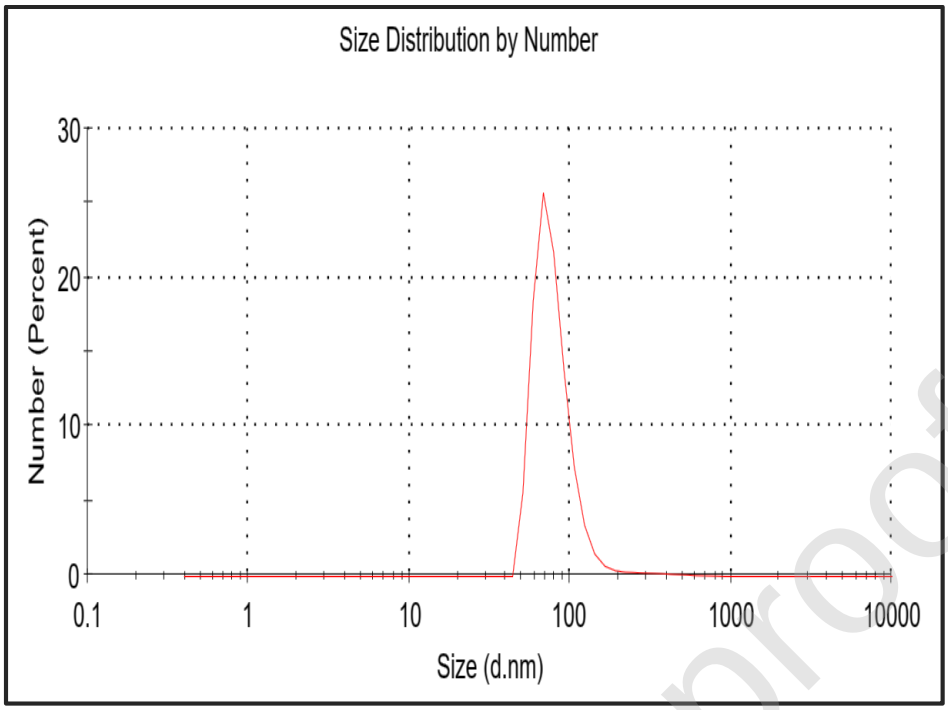

Fig. 1: Particle size distribution curve of **FONs-RSB**

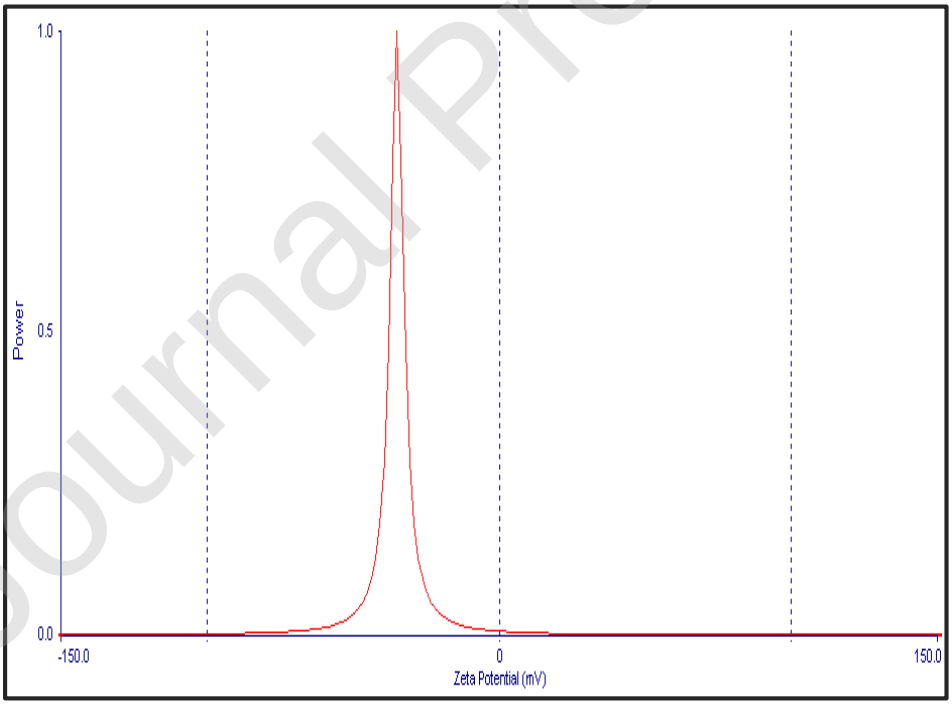

Fig. 2: zeta potential curve of **FON-RSB**

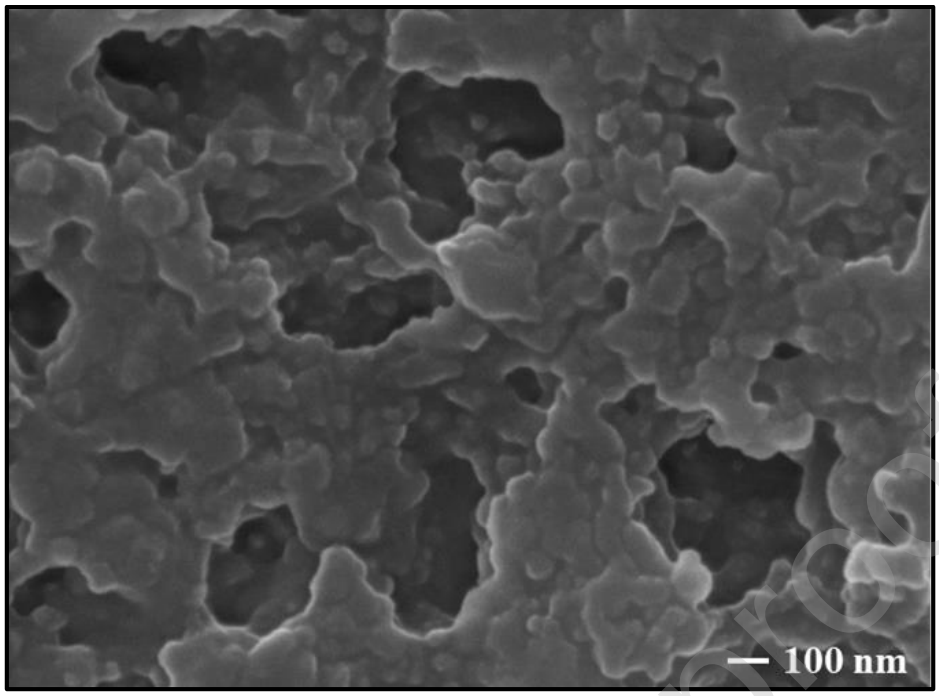

Fig. 3: Scanning electron microphotograph of **FONs-RSB**

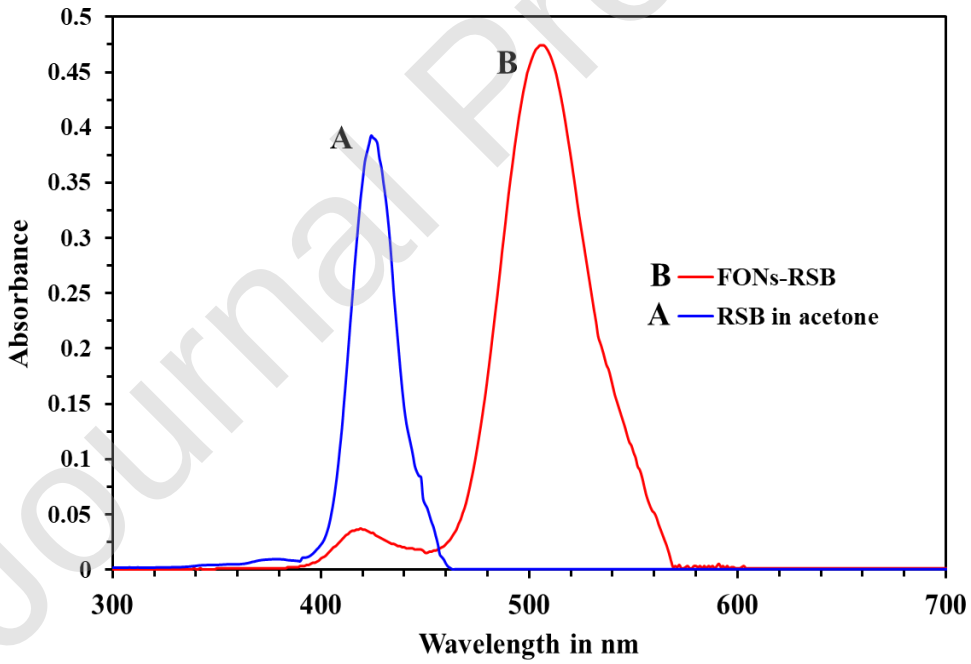

Fig. 4: Absorption spectrum of RSB in acetone [10 mM] (A) and aqueous suspension of **FONs-RSB** [50 µM] (B)

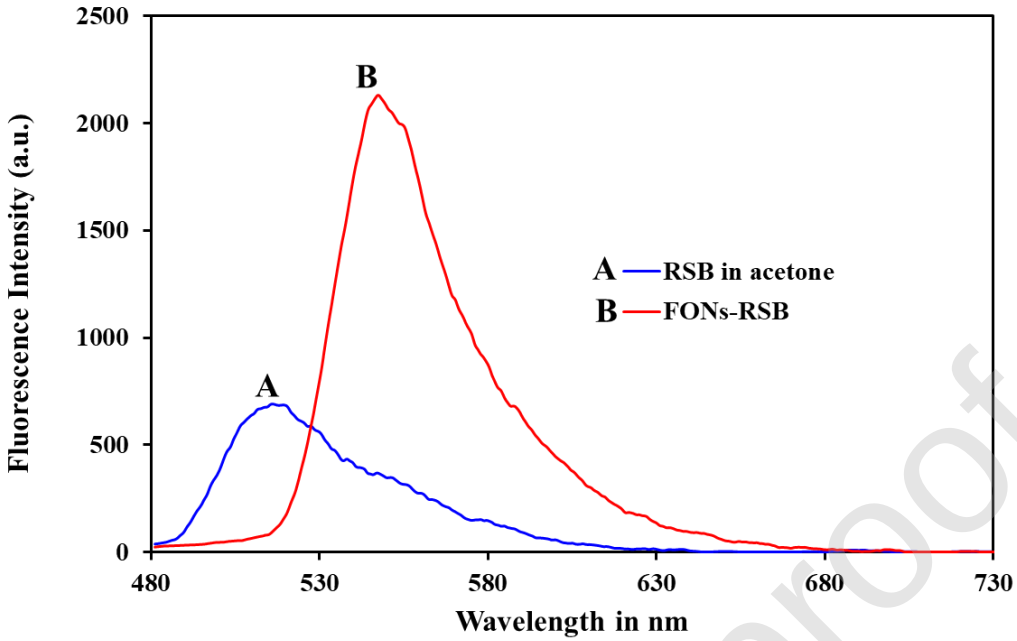

Fig. 5: Fluorescence spectra of RSB in acetone [10 mM] (A) and aqueous suspension of **FONs-RSB** [50 µM] (B)

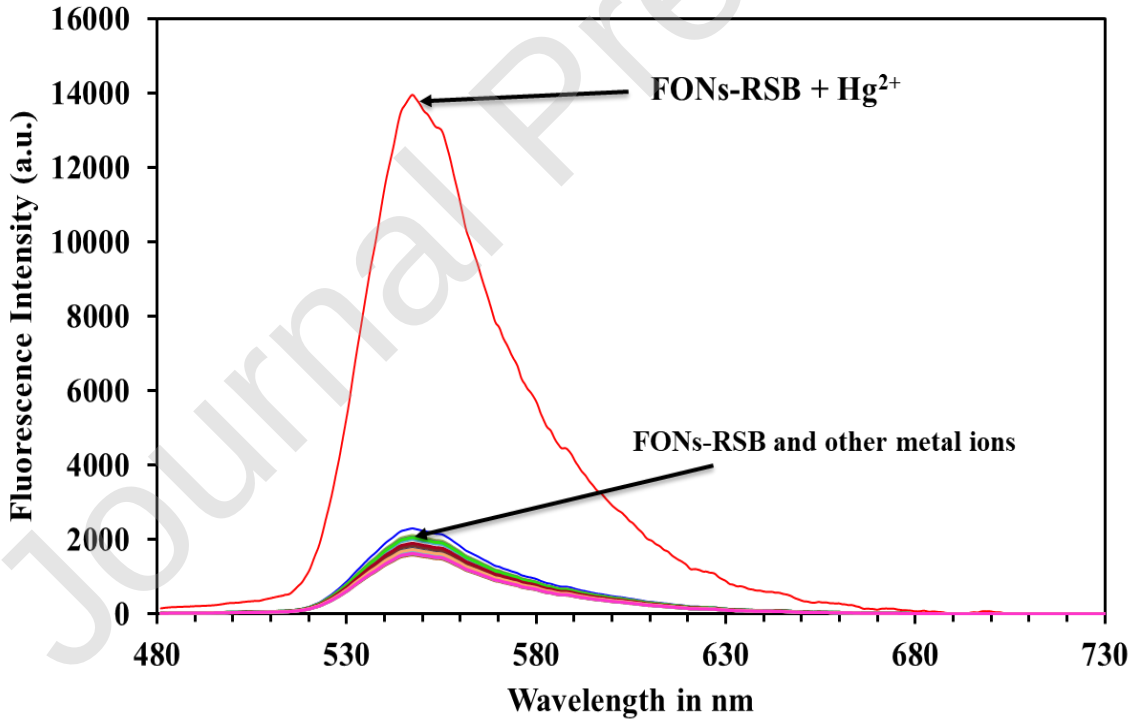

Fig. 6: Fluorescence emission spectra of **FONs-RSB** [50 µM] in the presence and absence of variety of positively charged metal ion solution [2 µg/mL]

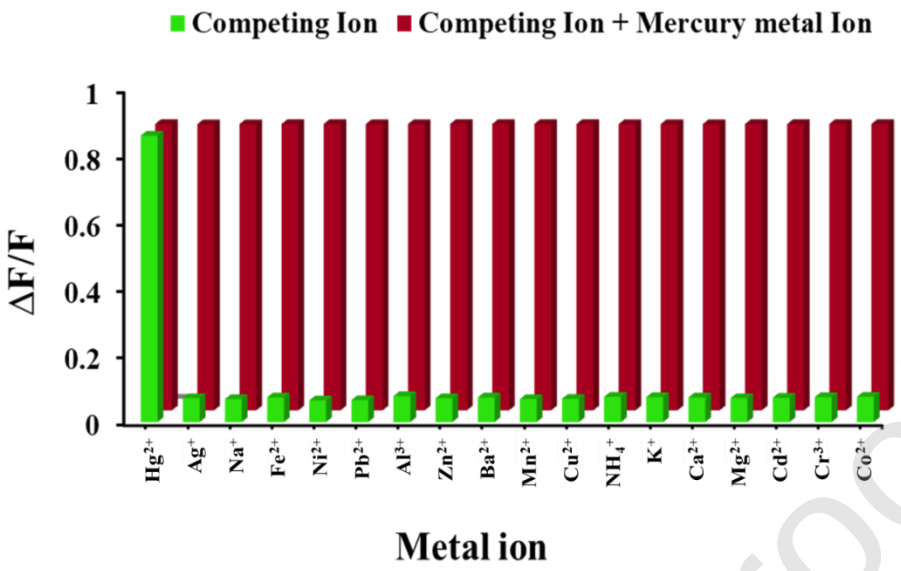

Fig. 7: Impact on change in the fluorescence intensity of **FONs-RSB** [50 µM] in the presence of each metal ion (green color bars, 2 µg/mL) and in the presence of Hg^{2+} along with foreign metal ions (brown color bars, 2 µg/mL)

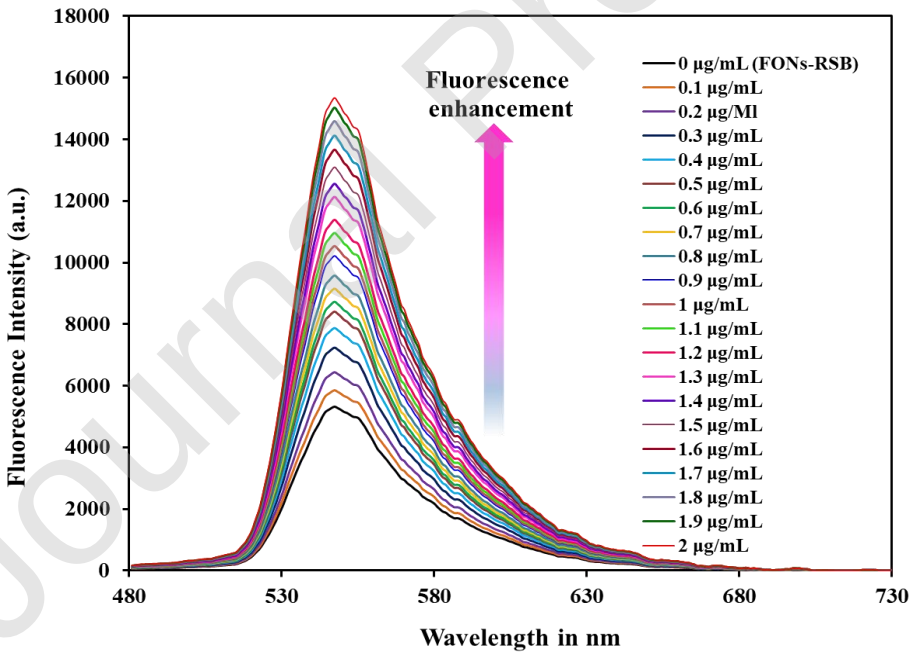

Fig. 8: Fluorescence intensity of **FONs-RSB** [50 µM] in the absence and presence of variable concentration of Hg^{2+} ion from 0 to 2 µg/mL

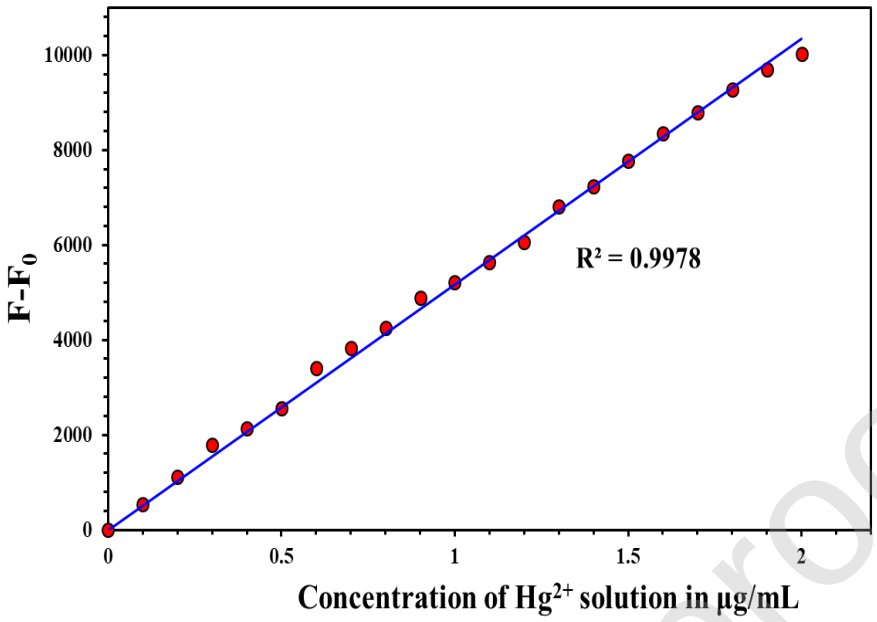

Fig. 9: Calibration plot for fluorescence enhancement of **FONs-RSB** [50 µM] by Hg^{2+} addition [0-2 µg/mL]

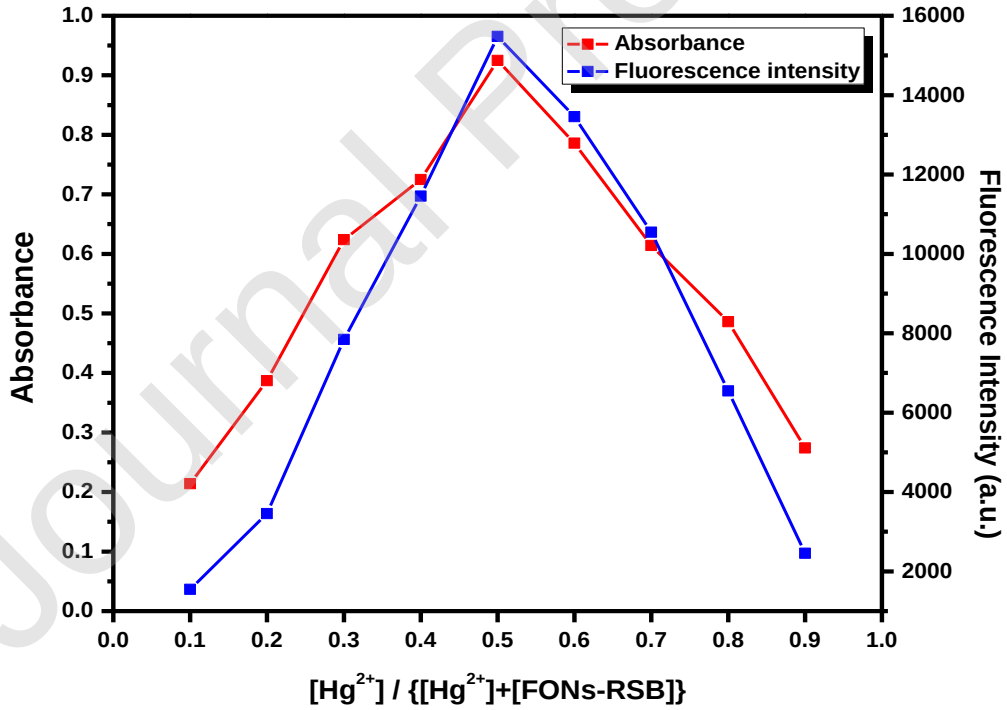

Fig. 10: Job's plot to investigate binding stoichiometry between **FONs-RSB** and Hg^{2+}

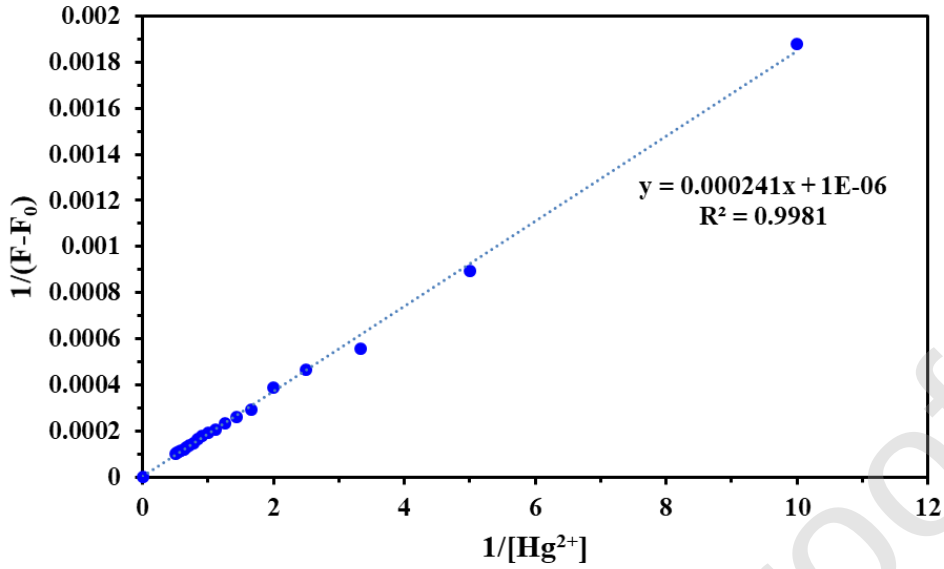

Fig. 11: Modified Benesi-Hildebrand Job's plot

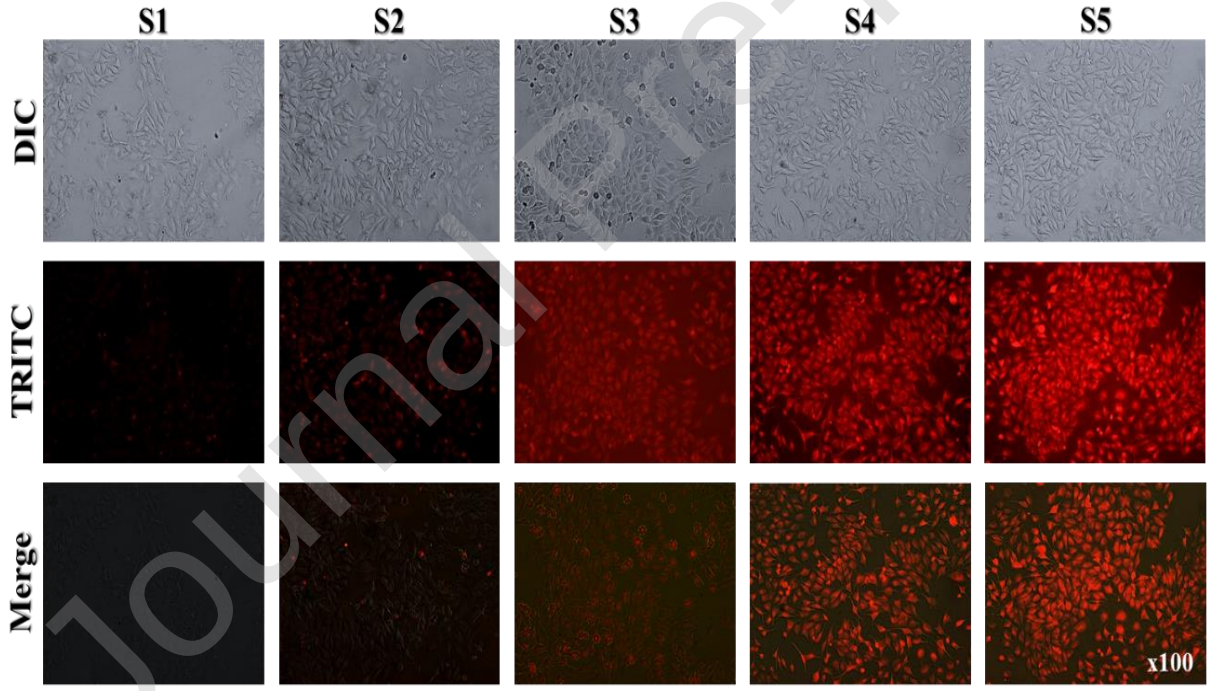

Fig. 12: Bright filed transmission images, fluorescence images exposed in green light 532 nm and merge images of living A375 cells with control (S1), RSB in acetone (S2) [10 mM], FONs-RSB (S3) [50 µM], FONs + 1 µg/mL Hg^{2+} (S4) and FONs-RSB + 2 µg/mL Hg^{2+} (S5)

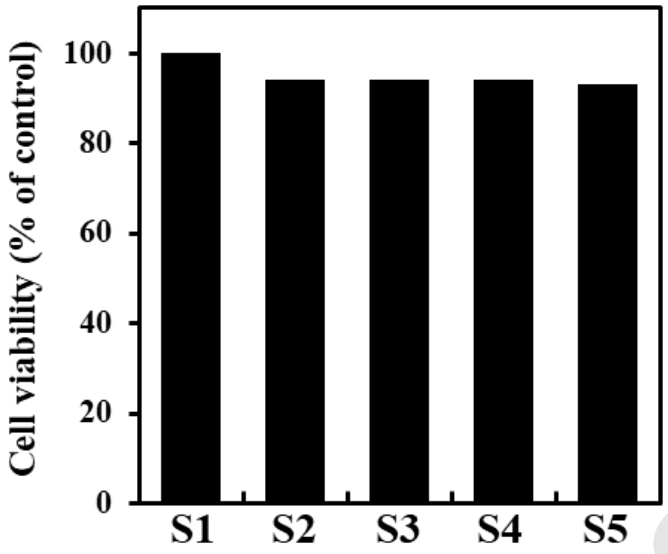

Fig. 13: Cell viability measurement using the MTT assay. A375 cells were untreated (Control-S1) and cells treated with RSB in acetone (S2) [10 mM], FONs-RSB (S3) [50 µM], FONs + 1 µg/mL Hg^{2+} (S4) and FONs-RSB + 2 µg/mL Hg^{2+} (S5) for 24 h.

Table 1: Comparison syntax of proposed fluorescent nanoprobe with already reported analytical methods and probes followed by their applicability in the determination of Hg^{2+}

Sr. No.	Method of analysis	Probe used for the detection	LOD	Real sample analysis	Ref. No.
1.	Colorimetric	Silver nanoparticles	0.85 µM	Tap/ Lake water	[4]
2.	Absorption spectroscopy	Anisotropic nanogolds	30 nM	Tap water	[24]
3.	Fluorescence	Rhodamine B derivative	30 nM	Bioimaging	[27]
4.	Spectrophotometry	Rhodamine derivative	77 nM	Digital information	[47]
5.	Colorimetric	Gold nanoparticles	50 nM	Pond/ River water	[48]
6.	Potentiometric	Gold nanoparticles	0.05 µM	Sewage water	[49]

7.	Electrochemical	Thiol functionalized reduced GO	0.2 µM	Tap water	[50]
8.	Amperometry	Modified carbon paste	2.5 µM	Natural water	[51]
9.	Conductometry	Cross linked BSA	0.025 µM	N.M.	[52]
10.	Colorimetric	Biosynthesized AuNPs	1.44 µM	N.M.	[53]
11.	Potentiometric	Chitosan -poly(vinyl alcohol) hydrogel film	1 nM	Industrial water	[54]
12.	Spectrophotometry	Ruthenium complex	0.1 µM	N.M.	[55]
13.	Potentiometric	Poly(vinyl chloride)	0.02 µM	Tap water	[56]
14.	Amperometry	Polyaniline-nafion nanostructure	0.05 µM	N.M.	[57]
15.	Fluorescence	Azo crown ether	13.9 µM	N.M.	[58]
16.	Fluorescence	GT capped AgNPs	0.037 nM	Tap/River water, Catalytic activity	[59]
17.	Fluorescence	BSA capped AuNPs	79 nM	Water samples	[60]
18.	Fluorescence	Azo dye	12.5 nM	Coal fired power plant water samples	[61]
19.	Fluorescence	Thiosemicarbazone	0.77 µM	N.M.	[62]
20.	Fluorescence	Thiol capped AuNPs	5 nM	N.M.	[63]
21.	**Fluorescence**	**Rhodamine based FONs**	**1.729 ng/mL (8.619 nM)**	**Tap/ River water and Intracellular cell imaging**	**Present work**

***N.M. = Not mentioned**

Table 2: Fluorescence lifetime values of **FONs-RSB** in the absence and presence of particular concentration of Hg^{2+} solution

Concentration of Metal ion Hg^{2+} added (µg/mL)	**Fluorescence lifetime value (τ) of FONs-RSB after addition of Hg^{2+} ion (ns)**
0	5.63
0.3	5.67
0.5	5.72
0.7	5.77
1.0	5.85
1.3	5.96
1.5	6.02
1.7	6.07

2	6.12

Table 3: Quantitative determination of the spiked quantity of Hg^{2+} in an environmental sample using the proposed method

water Samples Studied[#]	**Concentration of standard Hg^{2+} added (µg/mL)**	**Concentration of Hg^{2+} found (µg/mL) (n=3)**	**Recovery of Hg^{2+} (%)**	**Relative error (%)**
Tap Water	1	0.99	99.00	-0.0100
	1.5	1.49	99.33	-0.0067
	2	1.99	99.50	-0.0050
River Water	1	0.99	99.00	-0.0100
	1.5	1.48	98.66	-0.0134
	2	1.98	99.00	-0.0100

[*]**n** = Average of three determinations, [#] = Water samples collected from local campus near the university